CrystEngComm

Accepted Manuscript

ROYAL SOCIETY OF CHEMISTRY

www.rsc.org/crystengcomm

Four new metal–organic frameworks based on a rigid linear ligand: Synthesis, optical property and structural investigation

Chuanlei Zhang, Han Hao, Zhenzhen Shi and Hegen Zheng*

Dedicated to Professor Xinquan Xin on the occasion of his 80th birthday

Four coordination polymers, namely, $\{[Cd(L)(BIP)]\cdot 3H_2O\}_n$ (**1**), $\{[Co(L)(BIBP)(H_2O)_4]\cdot 4H_2O\}_n$ (**2**), $\{[Ni(L)(BIBP)(H_2O)_2]\cdot 2DMF\}_n$ (**3**), $[Ni(L)(BIMB)(DMF)(H_2O)]_n$ (**4**), have been synthesized based on a rigid linear carboxylate ligand (H_2L = 2',5'-dimethoxy-[1,1':4',1''-terphenyl]-4,4''-dicarboxylic acid) and different lengths of imidazole ligands (BIP = 1,4-di(1H-imidazol-1-yl)benzene; BIBP = 4,4'-di(1H-imidazol-1-yl)-1,1'-biphenyl; BIMB = 4,4'-bis((1H-imidazol-1-yl)methyl)-1,1'-biphenyl). These complexes have been characterized by single crystal X-ray diffraction, infrared spectroscopy, thermogravimetry, elemental analysis, and powder X-ray diffraction measurements. Complex **1** is a 6-connected 3-fold interpenetrating **pcu** net with point symbol $\{4^{12}\cdot 6^3\}$, **2** is a 1D supramolecular chain-like structure, **3** and **4** can be simplified as 4-connected **sql** nets with point symbol $\{4^4\cdot 6^2\}$. In addition, UV–visible spectra and photoluminescent properties are also investigated in detail.

Introduction

Current interest in metal–organic frameworks (MOFs) composed of inorganic and

State Key Laboratory of Coordination Chemistry, School of Chemistry and Chemical Engineering, Nanjing National Laboratory of Microstructures, Nanjing University, P. R. China

*E-mail: zhenghg@nju.edu.cn. Fax: 86-25-83314502

organic building units is rapidly expanding for their intriguing topologies and potential applications in selective molecular recognition and separation,[1] physical gas storage,[2] chemical absorption,[3] luminescence,[4] molecular magnet,[5] ion–exchange,[6] heterogeneous catalysis,[7] and so on. The rational design of coordination polymers is very challenging and depends on the advisable selection of linkers. Using hybrid linkers to construct MOFs is an important strategy in recent years.[8] Compared with flexible ligands, rigid ligands with desired geometry, have been more inclined to be used to specifically design topologies. Aromatic polycarboxylate linkers[9] and their derivate have been extensively utilized to synthesize various coordination polymers. Although unsubstituted carboxylate ligands have been studied comprehensively, less attention has been given to the methoxy–substituted polycarboxylate ligands. Introduction of methoxy groups in the aromatic polycarboxylates changes the planarity which has a significant effect on the final structure of coordination polymers.[10]

In this paper, we choose a rigid and symmetric ligand, 2',5'-dimethoxy-[1,1':4',1"-terphenyl]-4,4"-dicarboxylic acid (H_2L), which can potentially afford various coordination modes as well as diverse architectures. It is also capable of showing luminescence due to the presence of three phenyl rings. Moreover, different lengths of imidazole ligands (BIP = 1,4-di(1H-imidazol-1-yl)benzene; BIBP = 4,4'-di(1H-imidazol-1-yl)-1,1'-biphenyl; BIMB = 4,4'-bis((1H-imidazol-1-yl)methyl)-1,1'-biphenyl) also have been introduced to construct new structures. The aromatic dicarboxylate ligand incorporating imidazole ligands with M(II) (M = Cd, Co, Ni) ions under solvothermal conditions constructs four 1D, 2D or 3D metal–organic frameworks, namely, $\{[Cd(L)(BIP)]\cdot 3H_2O\}_n$ (**1**), $\{[Co(L)(BIBP)(H_2O)_4]\cdot 4H_2O\}_n$ (**2**), $\{[Ni(L)(BIBP)(H_2O)_2]\cdot 2DMF\}_n$ (**3**), $[Ni(L)(BIMB)(DMF)(H_2O)]_n$ (**4**) . All complexes are characterized by single crystal X-ray diffraction, infrared spectroscopy, thermogravimetry, elemental analysis, and powder X-ray diffraction measurements. Furthermore, crystal structures, topological analyses, UV–visible spectra and photoluminescent properties are investigated in detail.

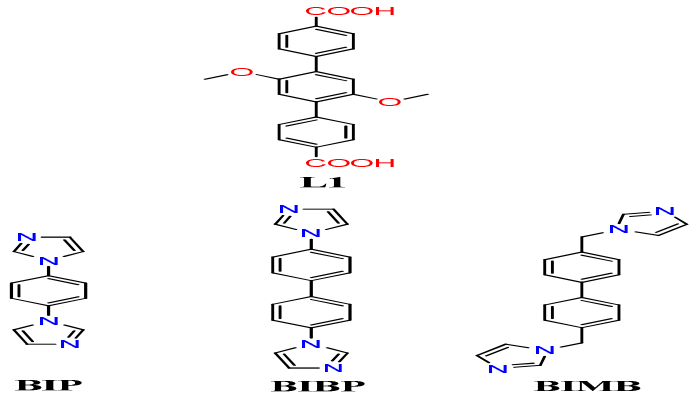

Scheme 1. Structures of the carboxylate ligand and imidazole ligands in this work

Experimental

Materials and methods

All chemicals and solvents except H_2L ligand were of reagent-grade quality from commercial sources and were used without further purification. The H_2L ligand was synthesized by the literature methods.[11] The IR absorption spectra of these complexes and H_2L ligand were recorded in the range of 400-4000 cm^{-1} by means of a Nicolet (Impact 410) spectrometer with KBr pellets. Element analyses (C, H, N) were carried out on a Perkin-Elmer model 240C analyzer. PXRD measurements were performed on a Bruker D8 Advance X-ray diffractometer using Mo Kα radiation (λ = 0.71073 nm), in which the X-ray tube was operated at 40 kV and 30 mA. Luminescent spectra were recorded with a SHIMAZU VF-320 X-ray fluorescence spectrophotometer at room temperature (25 °C). The decay lifetimes were measured with an Edinburgh Instruments FLS920P fluorescence spectrometer in the solid state at room temperature (RT). Solid-state UV-vis diffuse reflectance spectra was obtained at room temperature using Shimadzu UV-3600 double monochromator spectrophotometer, and $BaSO_4$ was used as a 100% reflectance standard for all materials. Thermogravimetric analysis (TGA) was performed under a N_2 atmosphere with a heating rate of 10 $K \cdot min^{-1}$ by using a Perkin-Elmer thermogravimetric analyzer.

Crystal structure determination

Single crystal X-ray data of complexes **1**–**4** were collected at 293 K on a Bruker SMART APEX CCD diffractometer using graphite monochromated Mo Kα radiation (λ = 0.71073 Å). The linear absorption coefficients, scattering factors for the atoms, and the anomalous dispersion corrections were referred to from the International Tables for X-ray Crystallography.[12] The structures were solved by direct methods, and the non-hydrogen atoms were located from the trial structure and then refined anisotropically using full-matrix least-squares procedures based on F^2 values using SHELXTL (version 6.10) crystallographic software.[13] The H-atoms of lattice DMF molecules in complex **3** and the H-atoms of coordinated water and DMF molecules in complexes **2**–**4** were located in difference Fourier maps. The H-atoms attached to carbon atoms were positioned geometrically and treated as riding atoms using SHELXL default parameters. Squeeze refinement was performed for complex **1** and **2** using PLATON[14] for their serious disorder, which shows three water molecules in **1** and four in **2**. The contribution of the solvent atoms has been incorporated in both the empirical formula and formula weight of complexes **1** and **2**. The crystal and refinement data are collected in Table 1. Selective bond distances and angles are given in Table S1 (Supporting Information). The topological analysis and some diagrams were produced using the TOPOS program.[15]

Synthesis of complexes 1-4

Synthesis of complex 1. A mixture of $Cd(NO_3)_2{\cdot}4H_2O$ (15.0 mg, 0.05 mmol), H_2L (18.9 mg, 0.05 mmol), and BIP (21.0 mg, 0.1 mmol) was dissolved in 6.0 mL of DMF/H_2O (4.5/1.5). The final mixture was placed in a Teflon vessel (15 mL) under autogenous pressure and heated at 95 °C for 3 days and then cooled to room temperature. Colourless crystals of **1** were collected in 46% yield (based on H_2L ligand). Elemental analysis calcd. for $C_{34}H_{32}N_4O_9Cd$ (%): C, 54.46; H, 4.12; N, 7.57. Found: C, 54.18; H, 4.25; N, 7.44. IR (KBr, cm^{-1}): 3443s, 1679s, 1585s, 1529vs, 1402vs, 1306m, 1210s, 1058s, 857m, 778m, 649m, 539m (Supporting Information Figure S6).

Synthesis of complex 2. A mixture of $Co(NO_3)_2{\cdot}6H_2O$ (14.55 mg, 0.05 mmol),

H_2L (18.9 mg, 0.05 mmol), and BIBP (28.6 mg, 0.1 mmol) was dissolved in 8.0 mL of DMF/H_2O (4.0/4.0). The final mixture was placed in a Teflon vessel (15 mL) under autogenous pressure and heated at 95°C for 3 days and then cooled to room temperature. The pink block crystals were obtained. Yield of the reaction was ca. 53% based on H_2L ligand. Elemental analysis calcd. for $C_{40}H_{46}N_4O_{14}Co$(%): C, 55.62; H, 5.20; N, 6.59. Found: C, 55.45; H, 5.31; N, 6.47. IR (KBr, cm^{-1}): 3446vs, 1608s, 1517s, 1384s, 1311s, 1214m, 1059m, 816m, 656w (Supporting Information Figure S7).

Synthesis of complex 3. A mixture of $Ni(NO_3)_2{\cdot}6H_2O$ (14.54 mg, 0.05 mmol), H_2L (18.9 mg, 0.05 mmol), and BIBP (28.6 mg, 0.1 mmol) was dissolved in 6.0 mL of DMF/H_2O (4.0/2.0). The final mixture was placed in a Teflon vessel (15 mL) under autogenous pressure and heated at 95 °C for 3 days and then cooled to room temperature. Green crystals of **3** were collected in 65% yield (based on H_2L ligand). Elemental analysis calcd. for $C_{46}H_{48}N_6O_{10}Ni$ (%): C, 60.88; H, 5.20; N, 9.44. Found: C, 61.06; H, 5.31; N, 9.29. IR (KBr, cm^{-1}): 3449vs, 1672vs, 1627vs, 1515vs, 1388vs, 1300m, 1212m, 1056s, 821s, 782w, 723w, 654w, 537w (Supporting Information Figure S8).

Synthesis of complex 4. A mixture of $Ni(NO_3)_2{\cdot}6H_2O$ (14.54 mg, 0.05 mmol), H_2L (18.9 mg, 0.05 mmol), and BIMB (31.4 mg, 0.1 mmol) was dissolved in 6.5 mL of DMF/H_2O (5.0/1.5). The final mixture was placed in a Teflon vessel (15 mL) under autogenous pressure and heated at 95 °C for 3 days and then cooled to room temperature. Green crystals of **4** were collected in 58% yield (based on H_2L ligand).. Elemental analysis calcd. for $C_{45}H_{43}N_5O_8Ni$ (%): C, 64.31; H, 4.98; N, 8.25. Found: C, 64.24; H, 5.12; N, 8.33. IR (KBr, cm^{-1}): 3439m, 1650vs, 1604vs, 1518m, 1389vs, 1210s, 1105s, 1051m, 1027m, 940w, 771w, 715w, 665m (Supporting Information Figure S9).

Results and discussion

Description of the crystal structure of $\{[Cd(L)(BIP)]\cdot 3H_2O\}_n$ (1)

Single crystal X-ray crystallographic analysis shows that complex **1** is a 3D supramolecular architecture with 3-fold interpenetration, crystallizes in the triclinic space group $P\bar{1}$. The asymmetric unit of **1** contains one Cd(II) ion, one L^{2-} ligand, one BIP ligand and three lattice H_2O molecules squeezed by PLATON software. Each Cd(II) is coordinated by four carboxylate oxygen atoms from three L^{2-} ligands in the equatorial plane, and two nitrogen atoms from two BIP ligands distribution in the axial position, which forms octahedral coordination geometry. The Cd–O bond distances are 2.301(5)–2.429(5) Å, and the Cd–N bond distances are 2.287(6) and 2.279(5) Å; the O–Cd–O angles are in the range of 54.32(19)–145.42(18)°, and the N–Cd–O angles are in the range of 83.7(2)–97.6(2)°, which are all similar to those values found in other Cd(II) complexes.[16]

Two crystallographically equivalent Cd(II) cations are bridged by two carboxylate groups adopting a bis-bidentate coordination mode to generate a dinuclear Cd(II) secondary building unit (SBU) with a Cd···Cd distance of 3.9448(6) Å (Figure 1a). Each dinuclear Cd cluster coordinates to four L^{2-} ligands to form a 2D layered network (Figure 1b), the diagonal size of this net is 23.118 × 36.064 $Å^2$. The BIP ligands link dinuclear Cd clusters in the axial position of the coordination octahedron further generate an infinite 3D framework (to see the framework clearly, "I" represents the BIP ligand) containing channels along the *a*, *b* and *c* axis (Figure 1c). These channels are filled by lattice water molecules.

A better insight into the nature of this intricate framework can be achieved by the application of a topological approach, reducing multidimensional structures to simple nodes and connection nets. The dinuclear Cd clusters can be regarded as 6-connected nodes and all crystallographical independent L^{2-} and BIP ligands acted as linkers. Therefore, the whole structure can thus be represented as a **pcu** net with the point symbol of $\{4^{12}\cdot6^3\}$ (Figure 1d). The potential voids are large to be filled via mutual interpenetration of an independent equivalent framework, generating a 3-fold interpenetrating 3D architecture (Figure 1e). Even with this interpenetration, the framework is still open, containing some 3D channels. Calculation with PLATON

shows that the effective volume for the inclusion is 21% of the crystal volume.

Description of the crystal structure of $\{[Co(L)(BIBP)(H_2O)_4]\cdot 4H_2O\}_n$ (2)

X-ray crystallographic analysis shows that complex **2** is a 1D supramolecular chain-like structure. The asymmetric unit contains two Co(II) ions, two L^{2-} anions, two BIBP ligands and eight coordinated water molecules and four lattice water molecules which are evident from the elemental analysis and thermogravimetric analysis. As shown in Figure 2a, each Co(II) is coordinated by four oxygen atoms from four coordinated water molecules and two nitrogen atoms from two BIBP ligands. The Co–O bond distances are in the range of 2.092(3)–2.133(3) Å, and the Co–N bond distances are vary in the range of 2.105(3)–2.129(3) Å; the O–Co–O angles are in the range of 88.10(11)–177.62(11)°, and the N–Co–O angles are in the range of 86.11(10)–95.06(12)°. The cobalt center with octahedral coordination is bridged by two BIBP ligands from nearly linear direction to form a 1D chain (Figure 2b).

Description of the crystal structure of $\{[Ni(L)(BIBP)(H_2O)_2]\cdot 2DMF\}_n$ (3)

X-Ray diffraction reveals that the asymmetric unit of **3** consists of two halves of Ni(II) ions both lying on an inversion centre, one L^{2-} ligand, one BIBP ligand, two coordinated water molecules and two solvent DMF molecules. The Ni(II) is defined by two nitrogen atoms and four oxygen atoms and adopts octahedral coordination geometry. The axial positions were occupied by two oxygen atoms from coordinated water molecules, and the equatorial plane consists of two nitrogen atoms from two BIBP ligands and two oxygen atoms from two L^{2-} ligands (Figure 3a). Two kinds of ligands coordinated to the Ni(II) ions to form a 2D rhombic grid with planar layers (Figure 3b). These layers are held together by different types of hydrogen bonding (d(O5···O4) = 2.5867(18) Å, ∠O5-H5B···O4 = 153°; d(O6···O3) = 2.7707(17) Å, ∠O6-H6C···O3 = 151°; d(C1···O5) = 3.343(7) Å, ∠C1-H1···O5 = 153°, etc.) and π···π stacking interactions (the distance between two parallel layers is 3.297 Å) in the structure to yield a 3D network.

One prominent structural feature of **3** is in the presence of channels formed by the accumulation of 2D layers. For a single 2D layer, the dimension of the rhombic grids is about 17.723 × 19.760 $Å^2$. Despite such a big cavity, the layers are non-interpenetrated. When the parallel layers are stacking in an AAA··· mode, as depicted in Figure 3c, infinite one-dimensional channels are created along the *a*-axis (Figure 3d). The solvent-accessible volume of these channels, calculated with the PLATON program, is 508.4 $Å^3$ or 23.9% of the total unit cell volume. These channels are occupied by many DMF solvent molecules, which have been crystallographically identified and well refined.

Description of the crystal structure of $[Ni(L)(BIMB)(DMF)(H_2O)]_n$ (4)

X-ray analysis reveals that complex **4** crystallizes in the orthorhombic space group *Pbcm*. Its asymmetric unit consists of half a Ni(II) ion on an inversion center, half a L^{2-} ligand, half a BIMB ligand, half a coordinated DMF molecule and coordinated water molecule (Figure 4a). Each Ni(II) is coordinated by two carboxylate oxygen atoms from two L^{2-} ligands, two nitrogen atoms from two BIMB ligands, one water and one DMF molecule, which forms the octahedral coordination geometry. The Ni–O bond distances are 2.0614(19) and 2.104(3) Å, and the Ni–N bond distances is 2.066(2) Å; the O–Ni–O angles are in the range of 85.95(8)–175.84(11)°, and the N–Ni–O angles are in the range of 87.19(9)–176.89(9)°, which are all similar to those values found in other Ni(II) complexes.[17] The imidazole groups of BIMB ligand link Ni ions to form a 1D linear chain, and the carboxylate groups of L ligands link these 1D chains with *zig-zag* direction to form a 2D network (Figure 4b). From a topological perspective, the octahedral coordinated Ni(II) center acts as a 4-connected node and complex **4** represents a $\{4^4 \cdot 6^2\}$ **sql** topology by using BIMB and L ligands as linkers (Figure 4d).

X-ray powder diffraction results

In order to check whether the crystal structures are truly representative of the bulk materials, the powder X-ray diffraction (PXRD) experiments for **1**–**4** were carried out

at room temperature. As shown in Figures S1–S4 (Supporting Information), the main peak positions of the simulated and experimental PXRD patterns are in agreement with each other.

UV–visible spectra

The UV–vis absorption spectra of H_2L and complexes **2**–**4** were carried out in the crystalline state at room temperature (Figure 5a). The H_2L ligand exhibits narrow absorption band in the range of 325–425 nm, which can be ascribed to π–π* transitions of the ligand. Besides this absorption band, complex **2** also has wide absorption band at 425–650 nm and complexes **3**–**4** at 525–775 nm**.** The lower energy bands can be considered as metal–to–ligand charge–transfer (MLCT) transitions. The higher energy band of **2** compared with **3** and **4** can be attributed to the spin–allowed d–d electronic transitions of the d^7 (Co^{2+}) cation.[18]

To explore the semiconductivity, the diffuse reflectivity is transformed into absorbance using the Kubelka–Munk function:[19]

$$F(R) = \frac{(1-R)^2}{2R} = \frac{K}{S}$$

with *R* representing the reflectance, *K* the absorption, and *S* the scattering. In a *K/S* vs *E* (eV) plot, extrapolating the linear part of the rising curve to zero provides the onset of absorption. As shown in Figure 5b, the band gap of H_2L is approximately 2.65ev, which exhibit the nature of semiconductivity.[20] The absorption band sites at 1.83 and 2.61 eV for **2**, 1.19 and 2.65 eV for **3**, 1.91 and 1.02 eV for **4**, respectively, which are estimated to be greater than the semiconductor silicon material with a band gap of 1.10 eV.

Luminescent properties

Complex **1** is insoluble in common organic solvents; so photoluminescence properties of **1** and free H_2L ligand were investigated in the solid state at room temperature (Figure 6). The free H_2L ligand exhibits an intense emission between 390 and 550 nm (λ_{max} = 450 nm upon excitation at 381 nm), which originated from charge transfer of

the internal H_2L ligand. The emission spectrum of complex **1** shows that the emission peaks center at 418 nm (λ_{ex} = 302 nm), which is blue–shifted 32 nm. Compared with the emission spectrum of H_2L, the origin of the broad and shifted emission band of complex **1** may be attributed to the coordination effect.[21] Because the Cd^{2+} ion is difficult to oxidize or reduce due to its d^{10} configuration, metal–to–ligand charge transfer (MLCT) and ligand–to–metal charge transfer (LMCT) are impossible essentially.

Furthermore, the emission decay lifetime of compound **1** was monitored. The luminescent decay curves (Supporting Information Figures 7–8) can be fitted with a double–exponential decay function. The emission lifetime values of complex **1** are lower than the corresponding values of H_2L ligand, indicating that the emission of **1** can be attributed to both the charge transfer of the internal H_2L ligand and the coordination effect. The emission decay lifetimes of **1** and H_2L ligand are as follows: H_2L ligand, τ_1 = 10.88 ns (51.44%), τ_2 = 1.75 ns (48.56%) (χ^2 = 1.055); complex **1**, τ_1 = 9.14 ns (47.65%), τ_2 = 1.37 ns (52.35%) (χ^2 = 1.122).

Thermogravimetric analyses

To estimate the stability of the coordination architectures, their thermal behaviors were studied by TGA (Supporting Information, Figure S10). For complex **1**, a weight loss of 7.36 % from ambient temperature to 210 °C can be ascribed to the loss of the lattice water (calcd 7.17 %), which were removed by the SQUEEZE routine in PLATON and were obtained by element analyses. Then the TG curve presents a platform and the framework starts to decompose at 290 °C. The weight loss of 8.41% for compound **2** before 120 °C corresponds to the loss of lattice water molecules (calcd 8.32%), which were removed by the SQUEEZE routine in PLATON and were obtained by element analyses. Then the curve presents a gravity platform until 308 °C, the sharply weightlessness represents the loss of coordinated water molecules (calcd 8.32%, found 8.24%). Followed by the structure gradually collapse. The TG curve of **3** shows a gradually weightlessness before 289 °C, is attributed to the loss of lattice DMF and coordinated H_2O molecules, then the curve presents a gravity platform.

After 350 ℃, a rapid weight loss is observed, which attributed to the decomposition of coordination framework. For complex **4**, there are two obvious weightlessness steps from 25 ℃ to 700 ℃. From 25 ℃ to nearly 200 ℃, the weight loss of 10.57% can be seen as the loss of coordinated DMF and H_2O molecules (calcd 10.85%). The second step starts from 315 ℃, the rapid weight loss can be seen as the burning of the organic ligands, at the same time accompanied by the collapse of the skeleton.

Conclusion

In summary, we have successfully synthesized and characterized four new compounds by the self-assembly of the rigid linear ligand H_2L, different lengths of imidazole ligands and different bivalent metal salts under solvothermal conditions. Compound **1** is a 6-connected 3-fold interpenetrating **pcu** net with point symbol $\{4^{12}\cdot6^3\}$. Although with multiple interpenetration, the framework is still open and large solvent accessible void space is up to 21%. Compound **2** is a 1D supramolecular chain-like structure. For H_2L ligand is uncoordinated and the framework has coordinated water molecules, the structure has a mass of hydrogen bonds, which can construct 2D hydrogen bonds networks. Compounds **3** and **4** can be simplified as 4-connected **sql** nets with point symbol $\{4^4\cdot6^2\}$. There are infinite one-dimensional channels in **3** when the parallel layers are stacking in an AAA··· mode. This structure feature does not appear in **4**, which may be caused by the different length of auxiliary ligands. In addition, the strong fluorescence emission and long emission lifetime of **1** display that it is promising phosphorescent material. UV–visible spectra of **2**–**4** indicate the nature of semiconductivity. Work is also underway to study that more MOFs with fascinating structures and interesting potential properties based on the semiconducting materials.

Acknowledgements

This work was supported by grants from the Natural Science Foundation of China

(Nos. 21371092, 91022011, 20971065) and National Basic Research Program of China (2010CB923303).

References

1 (a) B. L. Chen, S. C. Xiang and G. D. Qian, *Acc. Chem. Res*., 2010, **43**, 1115; (b) J. M. Roberts, B. M. Fini, A. A. Sarjeant, O. K. Farha, J. T. Hupp and K. A. Scheidt, *J. Am. Chem. Soc*., 2012, **134**, 3334; (c) F. Y. Yi, W. T. Yang and Z. M. Sun, *J. Mater. Chem.*, 2012, **22**, 23201; (d) L. E. Kreno, K. Leong, O. K. Farha, M. Allendorf, R. P. V. Duyne and J. T. Hupp, *Chem. Rev.*, 2012, **112**, 1105; (e) Z. Z. Lu, R. Zhang, Y. Z. Li, Z. J. Guo and H. G. Zheng, *J. Am. Chem. Soc*., 2011, **133**, 4172; (f) Y. Q. Lan, H. L. Jiang, S. L. Li and Q. Xu, *Adv. Mater*., 2011, **23**, 5015.

2 (a) D. P. Saha and S. G. Deng, *J. Colloid. Interf. Sci.*, 2010, **348**, 615; (b) M. Tagliabue, C. Rizzo, R. Millini, P. D. C. Dietzel, R. Blom and S. Zanardi, *J. Porous. Mat.*, 2011, **18**, 289; (c) D. J. Tranchemontagne, J. L. Mendoza-Cortes, M. O'Keeffe and O. M. Yaghi, *Chem. Soc. Rev*. 2009, **38**, 1257; (d) M. Yoshizawa, J. K. Klosterman and M. Fujita, *Angew. Chem. Int. Ed*., 2009, **48**, 3418; (e) S. Liu, D. H. Russell, N. F. Zinnel and B. C. Gibb, *J. Am. Chem. Soc*., 2013, **135**, 4314.

3 (a) S. Jakobsen, D. Gianolio, D. S. Wragg, M. H. Nilsen, H. Emerich, S. Bordiga, C. Lamberti, U. Olsbye, M. Tilset and K. P. Lillerud, *Phys. Rev. B*, 2012, **86**, 125429; (b) M. Muller, S. Hermes, K. Kaehler, M. W. E. van den Berg, M. Muhler and R. A. Fischer, *Chem. Mater.*, 2008, **20**, 4576; (c) K. V. Domasevitch, P. V. Solntsev, I. A. Gural'skiy, H. Krautscheid, E. B. Rusanov, A. N. Chernega and J. A. K. Howard, *Dalton Trans*., 2007, 3893; (d) S. Bordiga, E. Groppo, G. Agostini, J. A. Bokhoven and C. Lamberti, *Chem. Rev.*, 2013, **113**, 1736.

4 (a) C. Y. Su, Y. P. Cai, C. L. Chen, M. D. Smith, W. Kaim and H. C. Zur Loye, *J. Am. Chem. Soc*., 2003, **125**, 8595; (b) J. J. Perry, J. A. Perman and M. J. Zaworotko, *Chem. Soc. Rev.*, 2009, **38**, 1400; (c) Y. Zhang, J. Yang, Y. Yang, J.

Guo and J. F. Ma, *Cryst. Growth Des.*, 2012, **12**, 4060; (d) G. R. Desiraju, *J. Am. Chem. Soc*., 2013, **135**, 9952.

5 (a) K. Uemura, K. Y. Yamasaki, Y. Komagawa, K. Tanaka and H. Kita, *Angew. Chem. Int. Ed.*, 2007, **46**, 6662; (b) C. Streb, D. L. Long and L. Cronin, *Chem. Commun.*, 2007, 471.

6 (a) P. Mahata, A. Sundaresan and S. Natarajan, *Chem. Commun.*, 2007, 4471; (b) H. K. Chae, D. Y. Siberio-Perez, J. Kim, Y. B. Go, M. Eddaoudi, A. J. Matzger, M. O'Keeffe and O. M. Yaghi, *Nature*, 2004, **427**, 6974; (b) X. L. Wang, C. Qin, E. B. Wang and Z. M. Su, *Chem. Eur. J.*, 2006, **12**, 2680.

7 (a) M. A. Alam, A. Tsuda, Y. Sei, K. Yamaguchi and T. Aida, *Tetrahedron.*, 2008, **64**, 8264; (b) Q. F. Sun, J. Iwasa, D. Ogawa, Y. Ishido, S. Sato, T. Ozeki, Y. Sei, K. Yamaguchi and M. Fujita, *Science.*, 2010, **328**, 1144.

8 (a) Z. Q. Shi, Y. Z. Li, Z. J. Guo and H. G. Zheng, *Cryst. Growth Des.*, 2013, **13**, 3078; (b) X. Q. Yao, Z. R. Pan, J. S. Hu, Y. Z. Li, Z. J. Guo and H. G. Zheng, *Chem. Commun.*, 2011, **47**, 10049; (c) Z. J. Lin, T. F Liu, B. Xu, L. W. Han, Y. B. Huang and R. Cao, *CrystEngComm*., 2011, **13**, 3321.

9 (a) K. Koh, A. G. Wong-Foy and A. J. Matzger, *J. Am. Chem. Soc.*, 2009, **131**, 4184; (b) S. C. Jones and C. A. Bauer, *J. Am. Chem. Soc.*, 2009, **131**, 12516.

10 J. Sahu, M. Ahmad and P. K. Bharadwaj, *Cryst. Growth Des.*, 2013, **13**, 2618.

11 (a) K. Takaoka, M. Kawano, M. Tominaga and M. Fujita, *Angew. Chem., Int. Ed.,* 2005, **44**, 2151; (b) J. Seo, C. Bonneau, R. Matsuda, M. Takata and S. Kitagawa, *J. Am. Chem. Soc.*, 2011, **133**, 9005.

12 International Tables for X-Ray Crystallography; Kynoch Press:Birmingham, England, 1952; Vol. III.

13 SMART (version 5.0), SAINT-Plus (version 6), SHELXTL (version 6.1), and SADABS (version 2.03); Bruker AXS Inc.: Madison, WI.

14 Spek, A. L. PLATON; The University of Utrecht: Utrecht, The Netherlands, 1999.

15 V. A. Blatov, A. P. Shevchenko and V. N. Serezhkin, *J. Appl. Crystallogr.*, 2000, **33**, 1193.

16 (a) J. H. Luo, F. L. Jiang, R. H. Wang, L. Han, Z. Z. Lin, R. Cao and M. C. Hong,

J. Mol. Struct., 2004, 211; (b) C. H. Wei and K. B. Jacobson, *Inorg. Chem*., 1981, **20**, 356.

17 (a) J. S. Hu, Y. J. Shang, X. Q. Yao, L. Qin, Y. Z. Li, Z. J. Guo, H. G. Zheng and Z. L. Xue, *Cryst. Growth Des*., 2010, **10**, 4135; (b) B. Y. Li, G. H. Li, D. Liu, Y. Peng, X. J. Zhou, J. Hua, Z. Shi and S. H. Feng, *CrystEngComm*, 2011, **13**, 1291.

18 (a) D. Sarma, K. V. Ramanujachary, S. E. Lofland, T. Magdaleno and S. Natarajan, *Inorg. Chem*., 2009, **48**, 11660; (b) M. Tonigold, Y. Lu, A. Mavrandonakis, A. Puls, R. Staudt, J. Mo□llmer, J. Sauer and D. Volkmer, *Chem. Eur. J*., 2011, **17**, 8671; (c) B. K. Tripuramallu, P. Manna, S. N. Reddy and S. K. Das, *Cryst. Growth Des*., 2012, **12**, 777.

19 P. Kubelka and F. Z. Munk, *Tech. Phys*., 1931, **12**, 593.

20 (a) M. Alvaro, E. Carbonell, B. Ferrer, F. X. L. Xamena and H. Garcia, *Chem. Eur. J.*, 2007, **13**, 5106; (b) K. Maeda, M. Higashi, D. Lu, R. Abe and K. Domen, *J. Am. Chem. Soc*., 2010, **132**, 5858; (c) F. Hu, Q. G. Zhai, S. N. Li, Y. C. Jiang and M. C. Hu, *CrystEngComm.*, 2011, **13**, 414.

21 (a) S. Wang, *Coord. Chem. Rev.*, 2001, **215**, 79; (b) L. L. Wen, D. B. Dang, C. Y. Duan, Y. Z. Li, Z. F. Tian and Q. J. Meng, *Inorg. Chem.*, 2005, **44**, 7161.

Table 1. Crystal Data and Structural Refinements Parameters of Complexes 1–4

Complex	**1**	**2**	**3**	**4**
Empirical formula	$C_{34}H_{32}N_4O_9Cd$	$C_{40}H_{46}N_4O_{14}Co$	$C_{46}H_{48}N_6O_{10}Ni$	$C_{45}H_{43}N_5O_8Ni$
Formula weight	753	865.67	903.61	840.54
Crystal system	Triclinic	Monoclinic	Triclinic	Orthorhombic
Space group	$P\bar{1}$	$P2_1/c$	$P\bar{1}$	*Pbcm*
a / Å	9.4740(8)	22.625(2)	10.8266(7)	7.2985(4)
b / Å	11.2487(10)	14.9276(13)	12.4225(7)	16.4843(10)
c / Å	16.5633(15)	30.645(2)	16.9020(10)	34.438(2)
α / °	84.0930(10)	90.00	107.5810(10)	90.00
β/ °	89.4220(10)	128.963(4)	91.9470(10)	90.00
γ/ °	83.414(2)	90.00	99.3780(10)	90.00
V / Å^3	1744.2(3)	8047.6(11)	2129.7(2)	4143.3
Z	2	8	2	4
D_{calcd} / g cm^{-3}	1.331	1.310	1.409	1.344
μ / mm^{-1}	0.672	0.487	0.523	0.528
F(000)	708	3304	948	1752
θ min-max / °	1.24, 25.00	1.16, 27.52	1.75, 27.62	2.37, 27.59
Tot., uniq. data	12186, 6062	54676, 18268	19540, 9726	71648, 4888
R(int)	0.0791	0.0773	0.0384]	0.1190
Nref, Npar	6062, 408	18268, 1003	9726, 577	4888, 296
R_1, wR_2 [$I > 2\sigma(I)$]	0.0823,0.2205	0.0644, 0.1449	0.0438, 0.1212	0.0548, 0.1198
GOF on F^2	1.061	1.005	1.052	1.045
Min. and max resd dens (e·Å^{-3})	-2.748, 1.944	-0.533, 1.017	-0.977, 0.730	-0.364, 0.453

$R_1=\Sigma||F_o|-|F_c||/|\Sigma|F_o|$; $wR_2=\{\Sigma[w(F_o^2-F_c^2)^2]/\Sigma[w(F_o^2)^2]\}^{1/2}$; where $w=1/[\sigma^2(F_o^2)+(aP)^2+bP]$,$P=(F_o^2+2F_c^2)/3$.

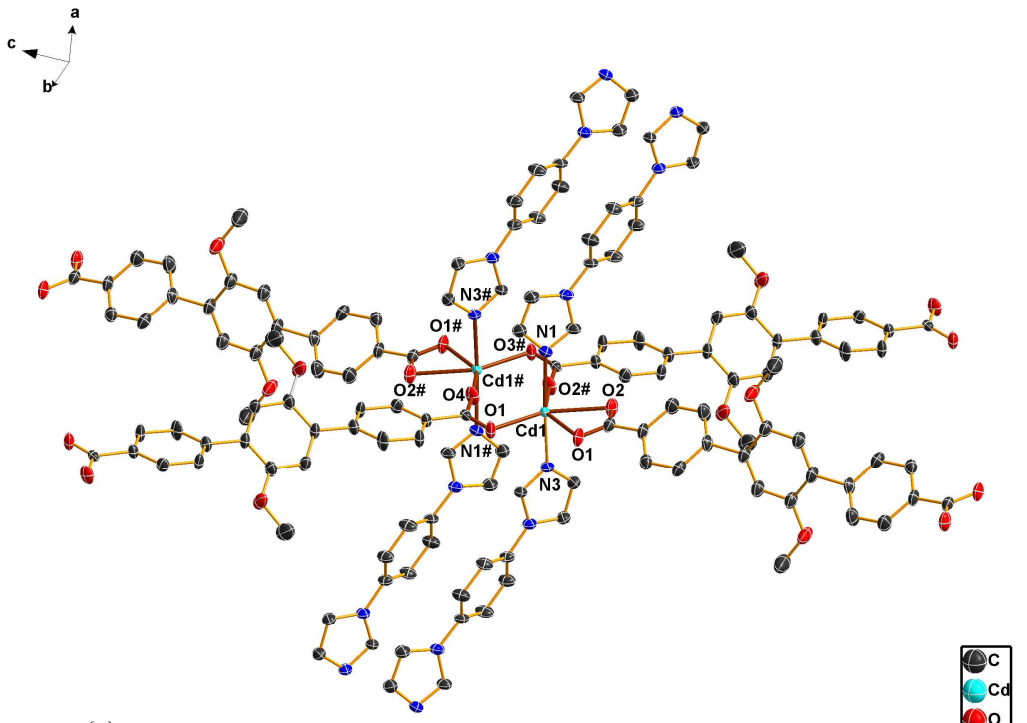

(a)

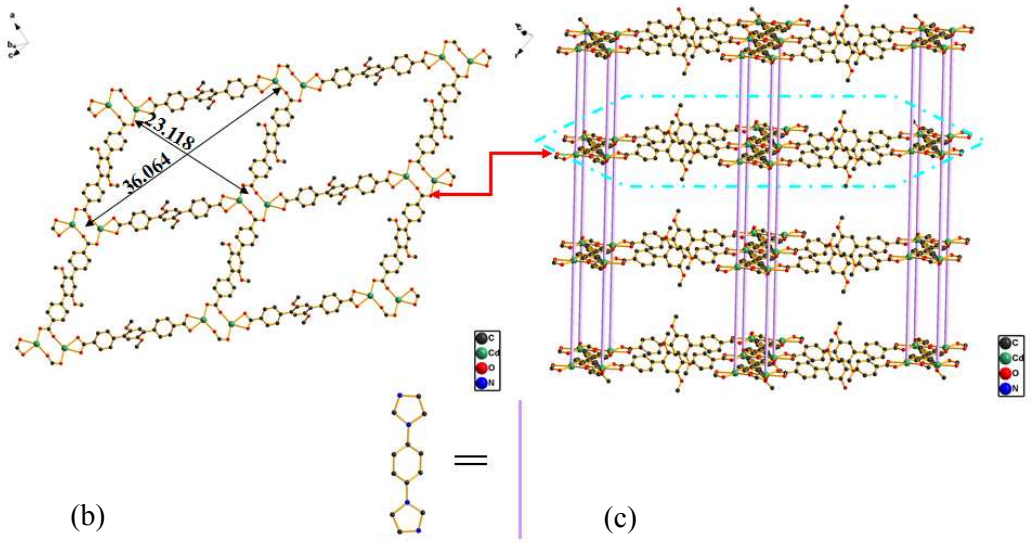

(b) (c)

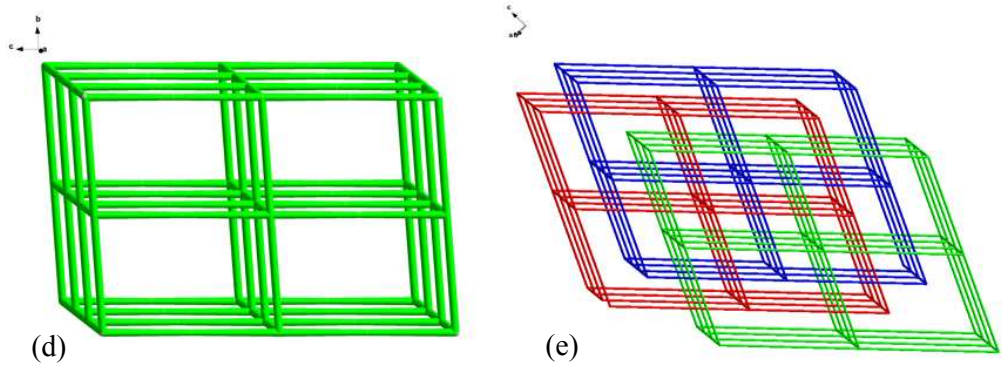

Figure 1. (a) Coordination environment of the dinuclear Cd(II) ions in **1**. The hydrogen atoms are omitted for clarity (30% ellipsoid probability). Symmetry codes: # 1 – *x*, 1 – *y*, 1 – *z*; (b) Views of the 2D network by L^{2-} ligands and Cd ions; (c) A perspective of 3D framework in **1**; (d) Schematic representation of a single 3D framework of **1**; (e) Views of 3-fold interpenetrating framework of **1**.

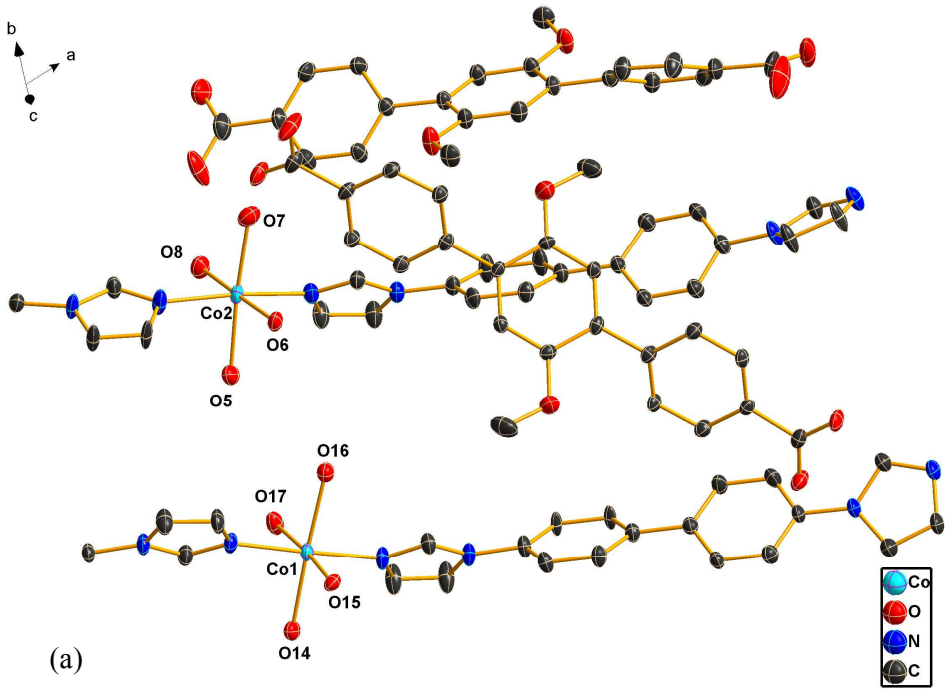

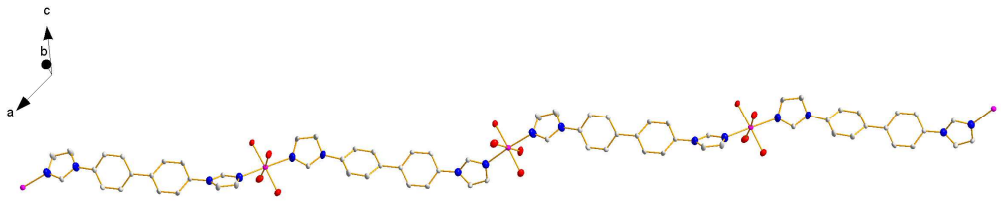

(b)

Figure 2. (a) Coordination environment of the Co(II) ions in **2**. The hydrogen atoms are omitted for clarity (30% ellipsoid probability). Symmetry codes: # = 1 + *x*, 1.5 – *y*, 0.5 + *z*; (b) The 1D chain constructed by BIBP ligands and Co(II) ions.

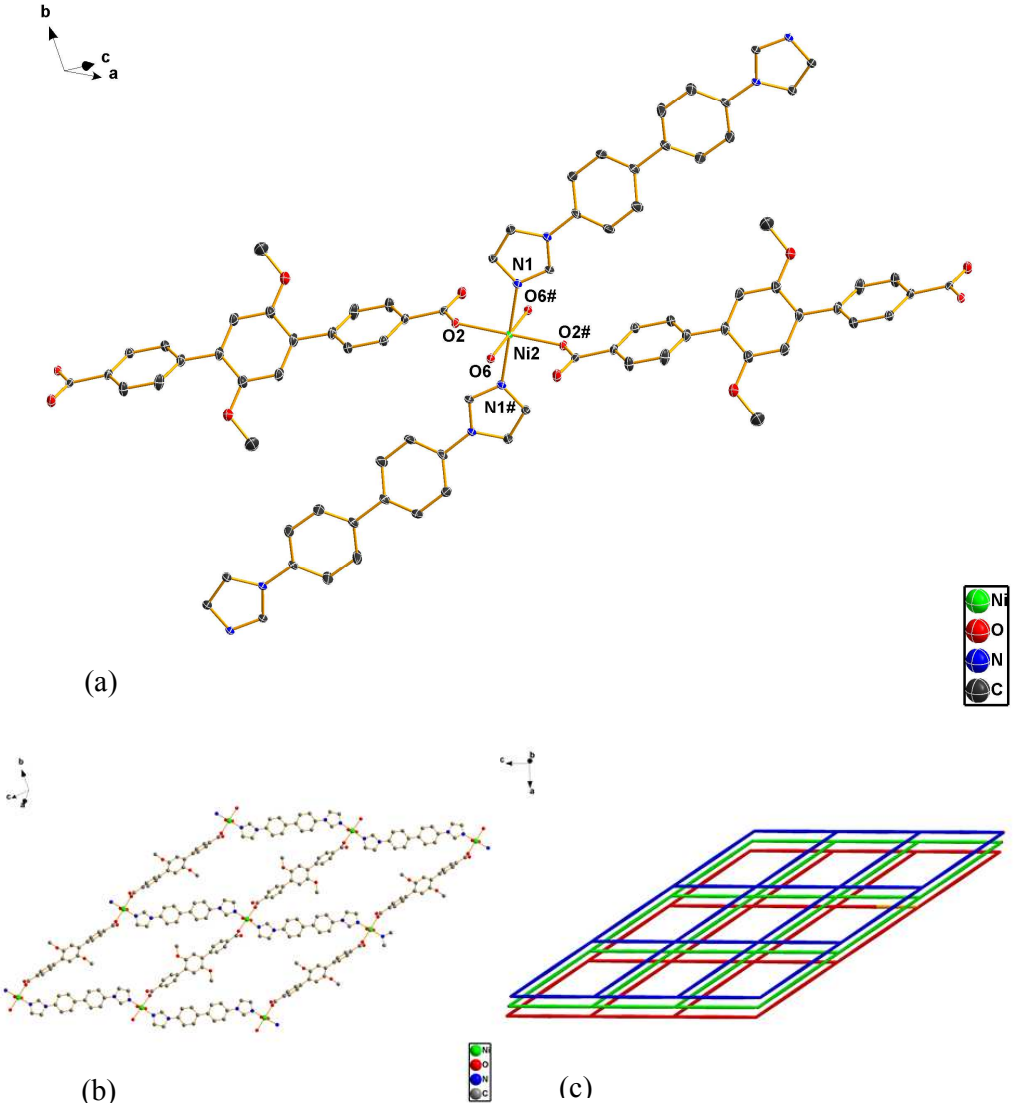

(a)

(b) (c)

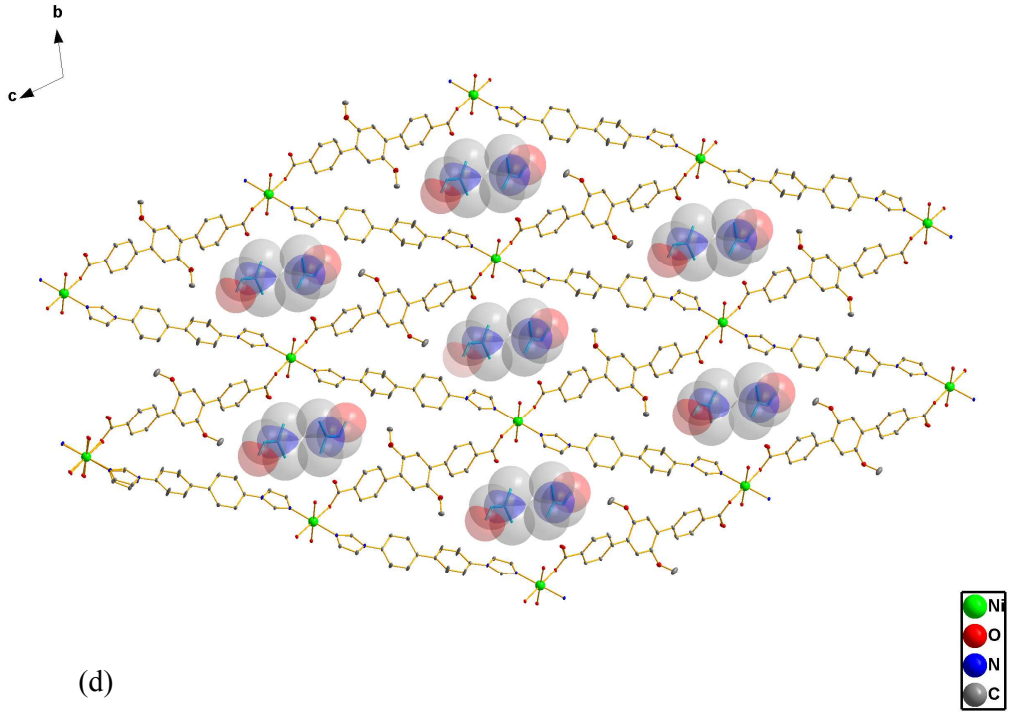

(d)

Figure 3. (a) Coordination environment of the Ni(II) ions in **3**. The hydrogen atoms and solvent molecules are omitted for clarity (30% ellipsoid probability). Symmetry codes: #1 = – *x*, –1 – *y*, – *z*; (b) The 2D rhombic grid of **3**; (c) The AAA···stacking 2D layers structure of **3**; (d) One-dimensional channels along the *a*-axis.

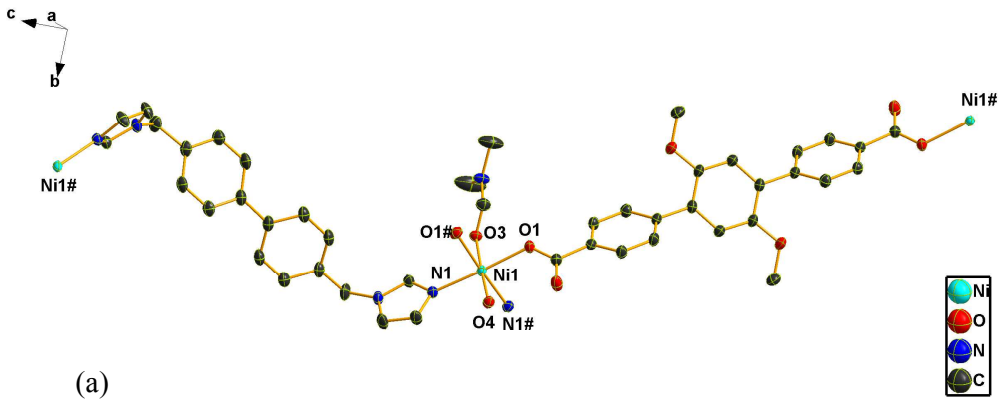

(a)

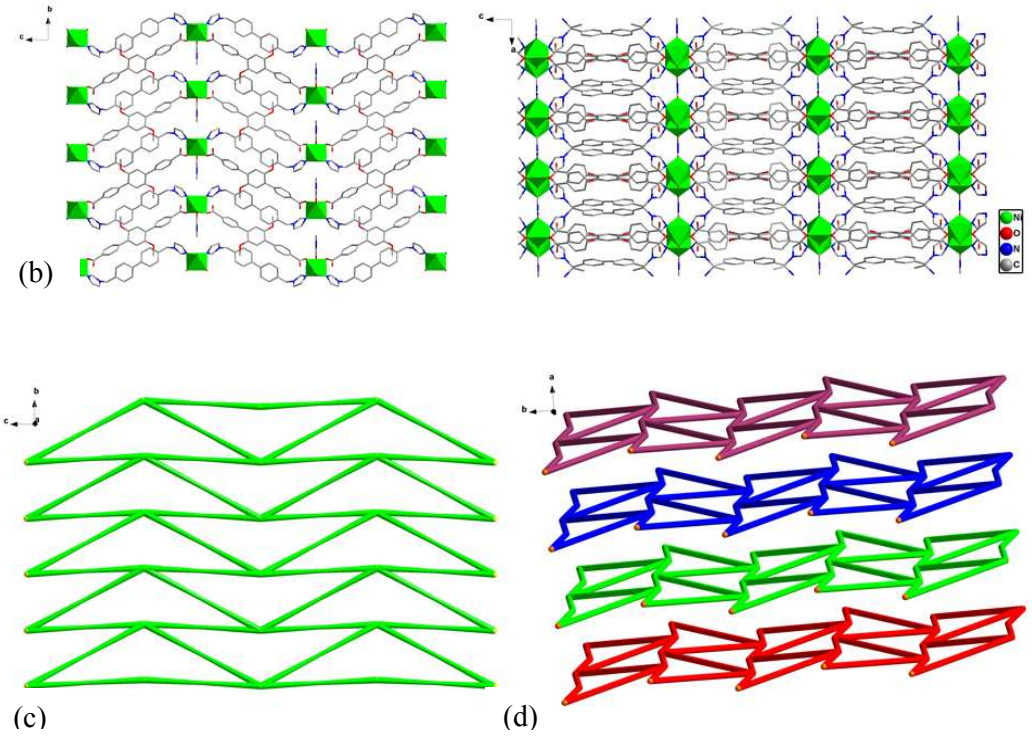

Figure 4. (a) Coordination environment of the Ni(II) ions in **4**. The hydrogen atoms and lattice solvent molecules are omitted for clarity (30% ellipsoid probability). Symmetry codes: # = *x*, *y*, 0.5 – *z*; (b) Perspectives of 2D structure along the *a* axis (left) and *b* axis (right); (c) Schematic representation of a single **sql** network; (d) The AAA···stacking 2D layers structure of **4**.

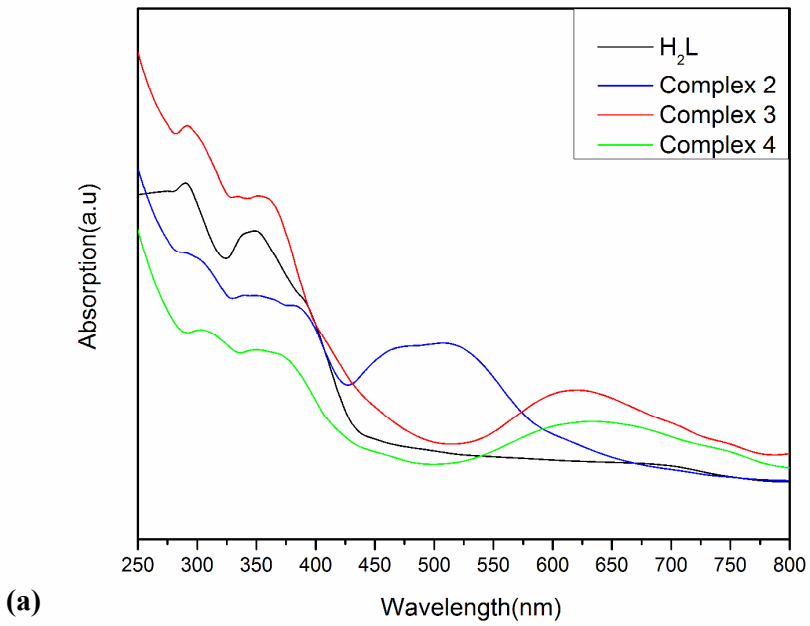

(a)

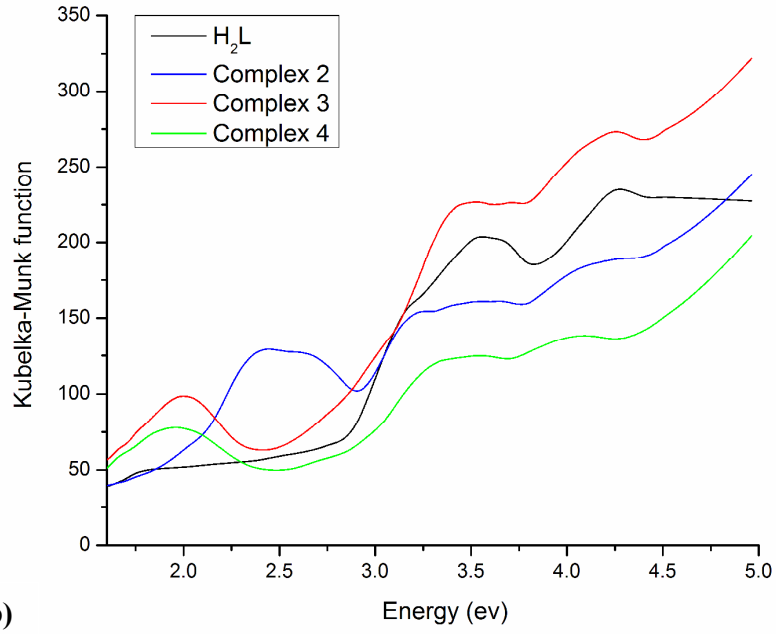

(b)

Figure 5. (a) UV-vis absorbance spectra and (b) Plot of Kubelka-Munk as a function of energy of **2 – 4** and corresponding ligand H_2L at room temperature.

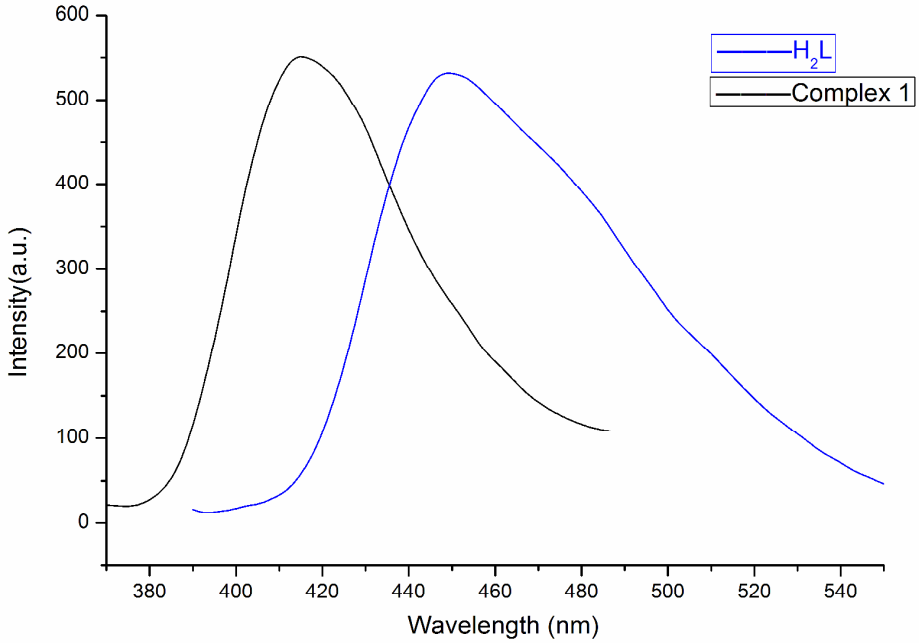

Figure 6. Solid-state photoluminescent spectra of **1** and H_2L ligand at room temperature.

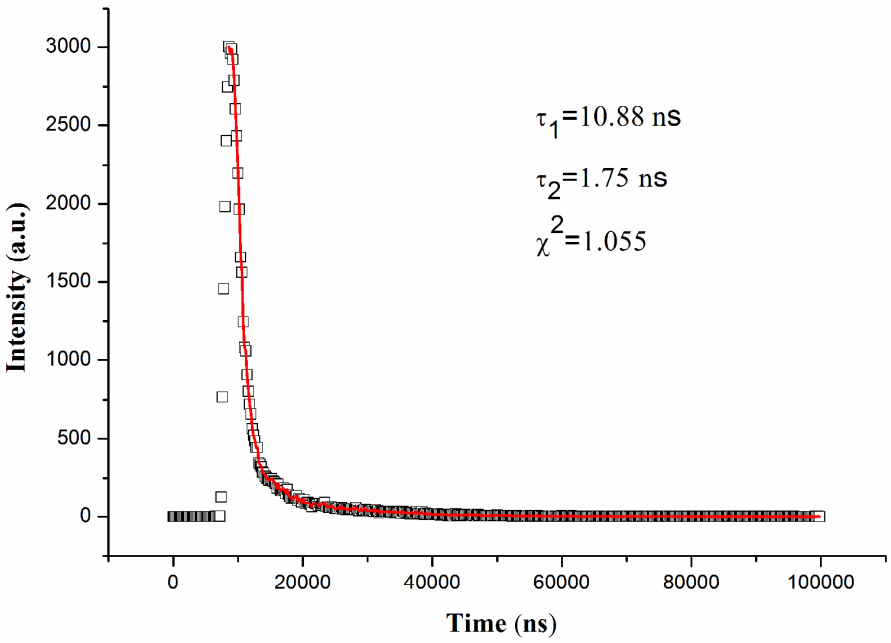

Figure 7. The fitted decay curve monitored at 450 nm for H_2L ligand in the solid state at room temperature. The sample was excited at381 nm. Blank circles: experimental data; Solid line: fitted by Fit = $A+B_1\times\exp(-t/\tau_1)+B_2\times\exp(-t/\tau_2)$.

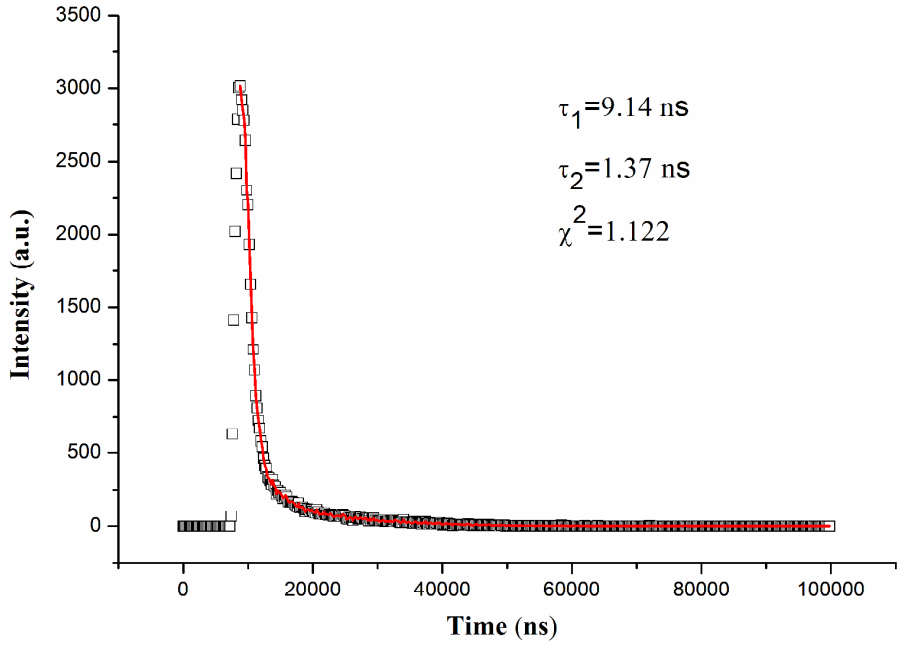

Figure 8. The fitted decay curve monitored at 418 nm for complex **1** in the solid state at room temperature. The sample was excited at 302 nm. Blank circles: experimental data; Solid line: fitted by Fit = $A+B_1\times\exp(-t/\tau_1)+B_2\times\exp(-t/\tau_2)$.